Chapter

Iron Oxide Nanoparticles: An Inorganic Phosphatase

Xiao-Lan Huang

Abstract

Phosphorus is one of the most important macronutrients for the primary production. The transformation of dissolved organic phosphorus in the environment and its contribution to biological production in the different ecosystems is still a mystery. Recently, it was demonstrated that phosphate ester can be rapidly hydrolyzed in solutions containing iron oxide nanoparticles with enzyme kinetics. The catalyst is sensitive to temperature and pH changes and inhibited by tetrahedral oxyanions with an order of $PO_4 < MoO_4 < WO_4$. The oxo-Fe structure in the iron oxide nanoparticles, like the metal center of natural phosphatase (e.g., purple acid phosphatase, PAP), might contribute to the observed catalytic activity. Iron oxide nanoparticles are very common and widely exist in the current earth environment, and phosphate esters are the main component of dissolved organic phosphorus in soil and waters. It is expected that iron oxide nanoparticles in aqueous environments, as an inorganic phosphatase, play a critical role for the phosphorus transformation from the view of the phosphorus cycle.

Keywords: enzyme, hydrolysis, iron oxide, nanoparticles, phosphate ester, phosphorus cycle

1. Introduction

Phosphorus is one of the most important macronutrients for the primary production, which is primarily taken up by plants in the form of phosphate ions (HPO_4^{2-} and $H_2PO_4^-$). Most of the knowledge of phosphorus in the environment, including the phosphorus geochemistry cycle, comes from inorganic phosphates [1–4]. The dissolved organic phosphorus transformation and its contribution to the biological production in the different ecosystems, e.g., soil, lake, estuary and ocean, is still a mystery [5–7]. Recently some limited works have indicated that different phosphate esters, especially monoesters are the main components in the dissolved organic phosphorus in soils [8–11] and waters [12–17], which might be an important source of P phytoavailability and a potential source of water eutrophication. The phosphomonoesters in supra-/macro-molecular structures were found to account for the majority (61–73%) of soil organic P in diverse agricultural soils across the world and the monoester P pool was estimated to account for 33% of the total phosphorus (587 ± 32 kg ha^{-1}) by a recently review [18].

In general, the phosphate ester hydrolysis is catalyzed by various enzymes, including purple acid phosphatases (PAPs), which have been identified and characterized from plant, animal and bacterial organisms [19]. On the other hand,

several studies have already demonstrated that the phosphate ester can be hydrolyzed with the interaction of minerals in the aqueous environments [5, 20–25]. Here, the results of laboratory study on the hydrolysis of phosphorus esters, promoted by the iron oxide nanoparticles in water, including the aged nanomolar inorganic iron ion solutions [26–28], were summarized. Additionally, the potential role of inorganic iron oxide nanoparticle for the phosphorus cycles due to the intrinsic phosphoesterase activity is postulated.

2. Promotion effect on the phosphate esters hydrolysis

Usually, phosphate ester in water is quite stable. As an example, hydrolysis Glucose 6-phosphate (G6P), a very common phosphate ester in nature, is a slow process without enzyme in the medium of deionized water (DIW), and becomes even slower in the fresh nanomolar inorganic iron solutions. Inorganic orthophosphate (P_i) in the DIW with the addition of 100 μM G6P at room temperature (22 ± 2°C) was initially 0.90 ± 0.04 μM, which became 4.86 ± 0.26 and 10.35 ± 1.19 μM at 4 and 12 days, respectively. The corresponding P_i in the fresh nanomole inorganic iron solutions (0.5–50 nM $Fe(NO_3)_3$) were 1.35 ± 0.09 and 2.55 ± 0.15 μM.

After G6P was added into an aged 14-month 16.5 nM $Fe(NO_3)_3$ solution (pH 6.30) at room temperature, made by acid-forced hydrolysis [27], the P_i was rapidly released (e.g. the initial 20 μM G6P, as presented in **Figure 1**). Like metal ions as well as natural and biomimetic enzymes, the kinetics of G6P hydrolysis in the aged iron solution can be described as a pseudo-first-order reaction for a fixed concentration of G6P [29–36]. For the initial 20 μM G6P, the decrease in G6P concentration, $[G6P]_t$, due to its hydrolysis can be expressed as a function of hydrolysis time, t, as

$$\log [G6P]_t = -1.31 \times 10^{-5} t - 4.718 \quad (r^2 = 0.999) \tag{1}$$

where $[G6P]_t$ is in M and t is in second.

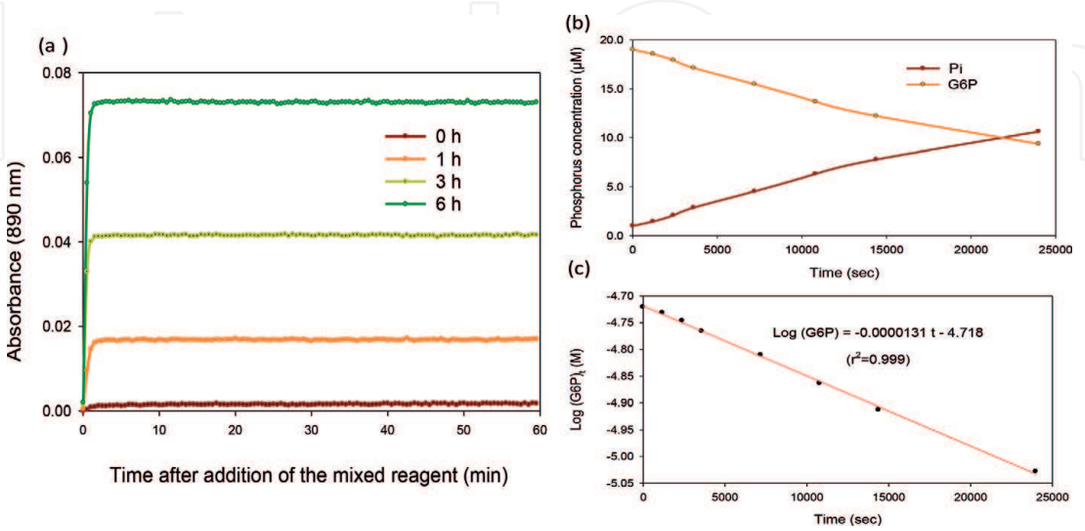

Figure 1.
Hydrolysis of 20 μM G6P in a 16.5 nM $Fe(NO_3)_3$ solution aged 14 months at room temperature (22 ± 2°C). (a) Time courses of formation of phosphorantimonylmolybdenum blue complex from phosphate released from hydrolysis of 20 μM G6P at times of 0, 1, 3, and 6 h, respectively; (b) concentration of P_i and G6P during G6P hydrolysis; and (c) pseudo first-order reaction kinetics of G6P.

The corresponding reaction rate constant (k) was 3.02×10^{-6} s^{-1}, and the half-life ($t_{1/2}$) was 6.38 h. Similar to the initial 20 μM of G6P, the P_i concentration of a initial 100 μM of G6P in the aged inorganic iron solution at 1, 3 and 6.7 h was 4.95, 10.74 and 20.62 μM, respectively. The corresponding k was 8.83×10^{-6} s^{-1}, and the $t_{1/2}$ was 21.8 h. It is highlighted that these k in the aged iron solution were much higher than the previously reported rates in the presence of the fresh unaged nanomolar inorganic iron [26] and millimole metals [30–32] solutions.

Like aged inorganic iron solution, the concentration of phosphate esters and condensed inorganic phosphate decreased, and inorganic orthophosphate (P_i) increased in a solution bearing iron oxide (IO) nanoparticles, which consists of a dialysis membrane tube (DMT, e.g., Spectra/Por 1 membranes, molecular weight cut-off (MWCO) 6000–8000 Da) filled with iron oxide (DMT-IO). The iron oxide (D) was synthesized by $Fe(NO_3)_3$ following the basic protocol of Atkinson [37] and aged at 80°C [28]. The k for 100 μM G6P, Glycerol-2-phosphate (3-carbon, G2P), and three energy metabolism compounds, i.e., adenosine monophosphate (AMP), adenosine diphosphate (ADP), adenosine triphosphate (ATP), as well as two inorganic condensed phosphates, i.e., polyphosphate (poly-P_i), and pyrophosphate (PP_i) at room temperature (22°C) was 2.69×10^{-5}, 1.68×10^{-5}, 1.54×10^{-5}, 5.73×10^{-6}, 5.76×10^{-6}, 3.8×10^{-6}, and 5.09×10^{-6} s^{-1}, respectively. The corresponding $t_{1/2}$ of these phosphorus esters and inorganic condensed phosphates was 7.1, 11.5, 12.5, 33.6, 33.4, 50.7, and 37.8 h, respectively.

Measured k of the initial 20 μM G6P with different sources of iron, either the aged inorganic iron solutions or the solutions bearing inorganic iron oxide nanoparticles (DMT-IO), are listed in **Table 1**. The half-life for aged 4-month Fe $(NO_3)_3$ (16.5 nM), $FeCl_3$ (10 nM) and $Fe(ClO_4)_3$(10 nM) was 37.8, 58.6 and 78.4 h, respectively, whereas the half-life of IO from the same source ($Fe(NO_3)_3$, JT Baker), aged at 5–80°C was 11, 2.7, 3.2 and 2.8 h, though they were in the same order of magnitude. The same patterns were observed for the ATP as well [28]. These results further indicate, as expected, that the behavior of catalysis depends on the sources of iron oxides nanoparticles in solutions—whether $FeCl_3$, or $Fe(NO_3)_3$, and even on the different manufacturers, as well as with the different aging temperatures for IO (5–80°C) [37, 38]. No clear relationships between ferric ion (III) sources, age processing, and catalytic activity, with the hydrolysis rate constant, were observed.

These inorganic iron solutions also have the same promotion effects on hydrolysis of different sugar phosphates, including G2P, ribose-5-phosphate (5-carbon, R5P), and fructose 1-phosphate (6-carbon, F1P) (**Table 2**). As expected, the promotion effect was also found on the hydrolysis of AMP, ADP and ATP, and inorganic condense phosphates (poly-P_i and PP_i) as well as the RNA model compound (4-nitrophenyl phosphate ester, pNPP). However, no promotion effects were observed for the hydrolysis of phosphonates (C-P bonded compounds, e.g., 2-aminoethylphosphonic acid, phosphono-formic acid) and inositol hexakisphosphate (IP6) (data not shown).

As expected, the catalytic activity is related to the soaked time of DIW with DMT-IO and the nature of IO, which can be described by the hydrolysis reaction rate constant. The kinetics of k of 100 μM G6P and ATP in three different IOs is presented in **Figure 2**. These results can be explained by the changes of the nanoparticles concentration in the water. It was expected that the concentration of the IO nanoparticles in these solutions would initially increase up to 10 days and then reach equilibrium. However, the total dissolved iron concentrations in these solutions were still beneath the detection limits of iron (0.1 nM) [39].

Fe source		Manufacturer	Aged time (mo.)	Aged temperature (°C)	IO nanoparticles or total Fe concentration (nM)	20 μM G6P	
						k (10^{-6} s^{-1})	$t_{0.5}$ (h)
Iron oxide nanoparticles (IO)	$Fe(NO_3)_3$	JT Baker	0.25	5	A	16.9	11
	$Fe(NO_3)_3$	JT Baker	0.25	22	B	70.3	2.7
	$Fe(NO_3)_3$	JT Baker	0.25	50	C	59.5	3.2
	$Fe(NO_3)_3$	JT Baker	0.25	80	D	106	1.8
	$FeCl_3$	JT Baker	0.25	25	E	13.8	14
	$Fe(NO_3)_3$	Riedel-de Haën	0.25	50	H	18.5	4.0
	$FeCl_3$	Riedel-de Haën	0.25	50	F	27.4	7.0
	$Fe(NO_3)_3$	Riedel-de Haën	0.25	80	L	80.7	2.4
	$FeCl_3$	Riedel-de Haën	0.25	80	G	54.1	3.6
Aged acidic forced hydrolysis inorganic Fe solution	$Fe(NO_3)_3$	JT Baker	14	22	16.5	30.17	6.4
		Riedel-de Haën	4	22	16.5	5.08	37.8
				22	100	2.96	65.6
			6	22	1000	18.77	10.3
	Iron standard solution (metal Fe in 0.3 M HNO_3)	JT Baker	4	22	1	2.38	81.0
					2.5	4.85	39.7
					7.5	7.22	26.7
					50	6.38	30.2
					100	6.55	29.4
					200	6.58	29.2
					500	8.14	23.6
					1000	5.86	32.8
	$FeCl_3$	JT Baker	16	22	2	6.59	29.2
					10	4.95	38.9
		Riedel-de Haën	4	22	10	3.28	58.6
					100	0.83	231.9
	$FeClO_4$	Aldrich	4	22	10	2.46	78.4
					100	0.61	318.3
	Fe $(NH_4)_2(SO_4)_2$	EM Science	16	22	16.5	9.49	20.3

[a] *The hydrolysis rate constant of 20 μM G6P in the DIW is 1.84 × 10^{-8} s^{-1}, and the corresponding half time is 10,450 h.*

Table 1.
Hydrolysis rate constant of 20 μM G6P in inorganic iron solutions.[a]

3. Kinetics of hydrolysis phosphate esters

As presented in **Table 2**, the hydrolysis reaction rate constant at different initial concentrations of phosphate esters in these aged inorganic iron salt solutions or inorganic iron oxides solutions were not constant. Surprisingly, the k from 5 to 250 μM G6P in the 16.5 nM $Fe(NO_3)_3$ solution aged for 14 months at room temperature

Phosphate ester	Fe source	Initial OP (μM)	Rate constant k (10^{-6} s^{-1})	Half-life $t_{0.5}$ (h)
Glycerol-2-phosphate (G2P)	Fe standard solution, 7.5 nM, 4 mo.	10	12.69	15.2
		20	6.4	30.1
		50	3.45	55.8
		500	0.51	374.3
	$Fe(NO_3)_3$, 1000 nM, 6 mo.	20	30.12	6.4
	$FeCl_3$, 2 nM, 16 mo.	20	5.29	36.4
	$Fe(NH_4)_2(SO_4)_2$, 16.5 nM, 16 mo.	20	11.44	16.8
	IO-D (made by $Fe(NO_3)_3$, aged a week at 80°C, soak 1 month at 22°C)	10	85.02	2.26
		50	26.91	7.15
		100	16.39	11.74
Ribose-5-phosphate (R5P)	Fe standard solution, 7.5 nM, 4 mo.	10	13.92	13.8
		20	8.15	23.6
	$Fe(NO_3)_3$, 1000 nM, 6 mo.	20	25.19	7.6
	$FeCl_3$, 2 nM, 16 mo.	20	7.24	26.6
	$Fe(NH_4)_2(SO_4)_2$, 16.5 nM, 16 mo.	20	16.16	11.9
Fuctose-1-phosphate (F1P)	Fe standard solution, 7.5 nM, 4 mo.	10	8.66	22.2
		20	5.25	36.4
	$Fe(NO_3)_3$, 1000 nM, 6 mo.	20	17.08	11.3
	$FeCl_3$, 2 nM, 16 mo.	20	5.29	36.4
	$Fe(NH_4)_2(SO_4)_2$, 16.5 nM, 16 mo.	20	8.5	22.6
Adenosine monophosphate (AMP)	IO-D (made by $Fe(NO_3)_3$, aged a week at 80°C, soak 1 month at 22°C)	10	79	2.44
		100	15.4	12.5
		250	6.2	31.1
Adenosine diphosphate (ADP)	IO-D (made by $Fe(NO_3)_3$, aged a week at 80°C, soak 1 month at 22°C)	10	134	1.44
		100	5.73	33.6
		250	1.59	121
Adenosine triphosphate (ATP)	IO-D (made by $Fe(NO_3)_3$, aged a week at 80°C, soak 1 month at 22°C)	10	61.5	3.13
		25	30.2	6.38
		100	4.4	43.8
	IO-A(made by $Fe(NO_3)_3$, aged a week at 5°C, soak 1 month at 22°C)	20	19.6	9.8
		100	10.8	17.9
	IO-B (made by $Fe(NO_3)_3$, aged a week at 22° C, soak 1 month at 22°C)	20	40.4	4.8
		100	8.46	22.7
	IO-G (made by $FeCl_3$, aged a week at 80°C, soak 1 month at 22°C)	20	38.7	5.0
		100	3.55	54.3
Polyphosphate (poly-P_i)	IO-D (made by $Fe(NO_3)_3$, aged a week at 80°C, soak 1 month at 22°C)	10	67.5	2.85
		100	3.8	50.7
		250	0.39	492
Pyrophosphate (PP_i)	IO-D (made by $Fe(NO_3)_3$, aged a week at 80°C, soak 1 month at 22°C)	10	162	1.19
		100	5.09	37.8
		250	0.71	270

Table 2.
Phosphate ester hydrolysis in the different inorganic iron solutions.

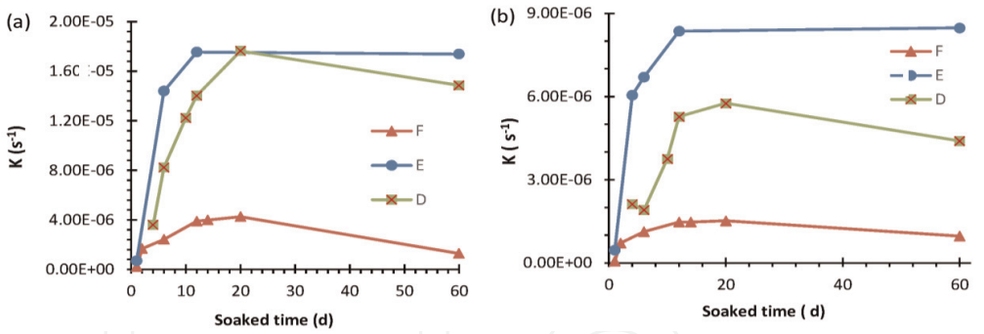

Figure 2.
Relationship between the soaked time of IO and hydrolysis rate of phosphorus in different DMT-IO solutions: (a) 100 μM G6P, and (b) 100 μM ATP (for details of IOs see ***Table 1****).*

can be further described by the Michaelis-Menten equation (**Figure 5a** and **b**), as the typical behavior of biocatalysts. This is contrast to previously reported promotion effects by metals [30–32, 40] and minerals [20, 22, 23, 41, 42]. The maximum k of G6P hydrolysis was about 1 nM s^{-1}, or 3.6 μM h^{-1}, and the Michaelis-Menten constant (K_m) was 13.7 μM of this aged inorganic iron solution.

$$\frac{1}{v} = 9.985 \times 10^{8} + \frac{1.371 \times 10^{9}}{[G6P]_o} \quad (r^2 = 0.997) \tag{2}$$

In fact, the promotion effect of G6P hydrolysis can be extended to 2500 μM in this aged iron solution with a k of 6.53×10^{-7} s^{-1}, and $t_{1/2}$ of 295 h. It should be pointed out that the concentration of total phosphorus in the solution was 10^3–10^5 higher than that of iron in the solution (e.g., 16.5 nM Fe and 2500 μM G6P).

The same patterns were also observed in the solution bearing inorganic iron oxide nanoparticles. Like the aged inorganic iron solution, the k of various organic phosphate esters or condensed phosphates at different concentrations were not

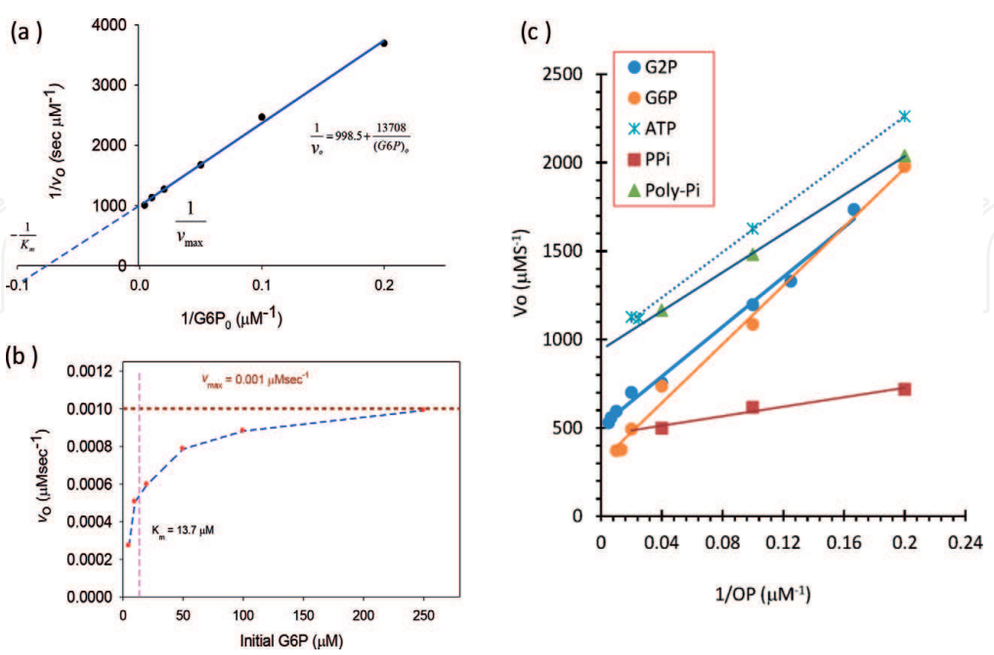

Figure 3.
Kinetics of hydrolysis of phosphate esters in inorganic iron solutions at room temperature (22 ± 2°C). (a) Double reciprocal (initial velocity and initial concentration of G6P) plot of G6P in the 14 month aged 16.5 nM $Fe(NO_3)_3$ solution, (b) initial velocity of G6P hydrolysis (v_o) as a function of the initial concentration of G6P in the aged iron solution, and (c) Lineweaver-Burk plot of different phosphate compounds in a DMT-IO solutions (IO-D).

Phosphorus source	V_m (nM S^{-1})	K_m (μM)	Range (μM)	r^2
G2P	2.0	7.0	6–200	0.99
G6P	3.2	8.3	5–100	0.99
ATP	0.9	9.2	5–50	0.99
Polyphosphate (poly-P_i)	1.1	5.5	5–25	1.00
Pyrophosphate (PP_i)	2.2	1.3	5–25	0.98

Table 3.
Michaelis-Menten constant (K_m) and maximum velocity (V_m) of different phosphorus in a DMT-IO solution (made by $Fe(NO_3)_3{\cdot}9H_2O$ and NaOH, aged a week at 80°C, IO-D, soaked a month).

constant (**Table 2**). The catalytic activity of the different concentration of phosphorus also can be described by the typical Michaelis-Menten equations (**Figure 3c**). Based on the Lineweaver-Burk linear equation ($1/V$ is a linear function of $1/[S]$), the Michaelis-Menten constant (K_m) and maximum velocity (V_m), as well as the range of concentration of phosphorous among these compounds, were determined (**Table 3**). Meanwhile, the catalysis activity was still observed even when the total phosphorus esters exceeded the range of the Michaelis-Menten equations, as with many of the natural enzymes, including the PAP [43].

It should further be pointed out that the similar enzyme kinetics (Michaelis-Menten equations) were observed recently by many inorganic nanoparticles studies, which have been described as nanozyme [44–47]. For example, Fe_3O_4 [44], α-Fe_2O_3 [48], γ-Fe_2O_3 [49], γ-FeOOH [50], Co_3O_4 [51], $MnFe_2O_4$ [52, 53], MFe_2O_4 (M = Mg, Ni, Cu) [54], $ZnFe_2O_4$ [55], NiO [56], and MnO_2 [57] have been observed to have peroxidase-like or catalase-like activity, whereas the vanadium pentoxide (V_2O_5) was demonstrated to have antioxidant enzyme-like (glutathione peroxidase) activity [58–61] and molybdenum trioxide (MoO_3) nanoparticles to have sulfite oxidase activity [62].

4. Inhabitation effects of tetrahedral oxyanions

The hydrolysis of phosphorus ester was significantly inhibited when the tetrahedral oxyanions were introduced into inorganic iron oxides nanoparticle solution, e.g., G6P in a 10-month aged iron solution (**Figure 4**), as the natural PAPs. Both the catalytic and the inhibition behaviors of the catalysis in the presence of 5–125 μM G6P with different tetrahedral oxyanions can be described by a Michaelis-Menten equation (Eqs. (3)–(7)) as follows:

$$\text{without any addition}: \frac{1}{v} = 7.4 \times 10^8 + \frac{2.001 \times 10^9}{[\text{G6P}]_o} \quad \left(r^2 = 0.945\right) \tag{3}$$

$$\text{with } 1\ \mu M\ \text{MoO}_4: \frac{1}{v} = 7.4 \times 10^8 + \frac{1.044 \times 10^{10}}{[\text{G6P}]_o} \quad \left(r^2 = 0.998\right) \tag{4}$$

$$\text{with } 1\ \mu M\ \text{WO}_4: \frac{1}{v} = 7.4 \times 10^8 + \frac{3.423 \times 10^{10}}{[\text{G6P}]_o} \quad \left(r^2 = 0.995\right) \tag{5}$$

$$\text{with } 5\ \mu M\ \text{PO}_4: \frac{1}{v} = 7.4 \times 10^8 + \frac{8.317 \times 10^9}{[\text{G6P}]_o} \quad \left(r^2 = 0.988\right) \tag{6}$$

$$\text{with } 10\ \mu M\ \text{PO}_4: \frac{1}{v} = 7.4 \times 10^8 + \frac{1.216 \times 10^{10}}{[\text{G6P}]_o} \quad \left(r^2 = 0.997\right) \tag{7}$$

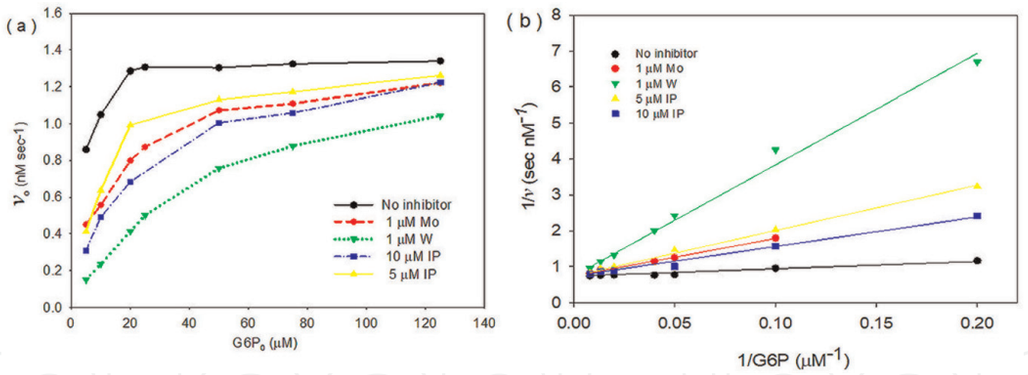

Figure 4.
Inhibiting behavior of different tetrahedral oxyanions on the hydrolysis of Glucose-6-phosphate in an aged 10-month, 1000 nM $Fe(NO_3)_3$ solution at room temperature (22 ± 2°C). (a) Effect of initial concentration of G6P on the initial hydrolysis velocity of G6P, and (b) Lineweaver-Burk plot of aged iron solution in the absence and presence of tetrahedral oxyanions.

The results indicated that the catalysis sites from these catalyst, i.e., the inorganic iron oxide nanoparticles, may be only bound to either the tetrahedral oxyanions (PO_4, MoO_4, and WO_4) or phosphate esters to form an intermediate, but cannot bind both of them at any given moment. The modes of tetrahedral oxyanions and G6P are competitive (**Figure 5**). The K_m, the G6P concentration at which the reaction rate reaches one-half of maximum velocity ($v_{max}/2$), was about 2.7 μM G6P in this aged iron solutions with no inhibitors. The K_{Mapp} with addition 1 μM WO_4, MoO_4, and 5 and 10 μM PO_4 was 46.2, 14.1, 11.1 and 17.1 μM G6P, respectively. Therefore, the K_i of WO_4, MoO_4, and PO_4 are 0.06, 0.24 and 1.6–1.9 μM, respectively. It is interesting to compare the catalytic behavior of these inorganic iron oxides nanoparticles solution to natural PAPs and their biomimetics, though the velocities of hydrolysis G6P in the inorganic catalyst are still lower than that of natural phosphoesterase. For natural PAPs, K_m and K_i of PO_4 is usually in the millimolar range [63–69], only K_i of WO_4 and MoO_4 is in the micromolar range [65, 66, 70–72]. The value of K_m of G6P is 920 μM for PAP extracted from sweet potato [33] and 300–310 μM for those from soybean seed [73]. Besides, the modes

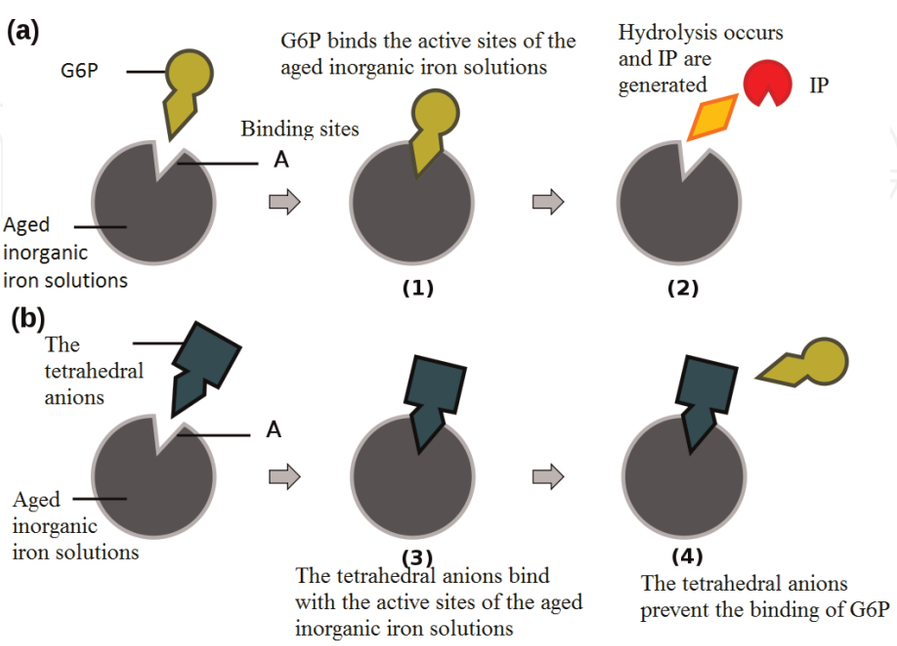

Figure 5.
Diagram of catalysis process of G6P hydrolysis in the presence of the tetrahedral anions in the aged inorganic iron solutions. (a) Reaction without tetrahedral anions; (b) Inhibition with the competitive tetrahedral anions.

of molybdate and tungstate inhibition are noncompetitive [65, 66, 70–74]. Only orthophosphate for natural PAPs are competitive [65, 66] in most cases.

A more significant difference between the inorganic catalyst and the natural phosphoesterase is revealed in their response to the fluoride ion. The activity of all known natural phosphoesterase is very sensitive to fluoride, even at the micromolar level [67, 72–78], while the catalytic activity of the inorganic iron oxides solutions still remain, even when the final concentration of fluoride in the solutions were up to 0.5 M.

5. Effect of temperature

The catalyst on the hydrolysis of phosphate ester is sensitive to temperature, as natural enzymes. The optimum temperature for the phosphate ester hydrolysis reaction by these inorganic catalysts was around 50°C (**Figure 6**), which is comparable to recent observations on the natural enzymes [79–82]. However, catalytic activity of the IO nanoparticles in solution was lost as the temperature was raised to 90°C for an hour or to 72°C for 16 h. This behavior is similar to the thermal denaturation of the natural enzyme. Moreover, the temperature coefficient, Q_{10}, a measure of the hydrolysis velocity, is also decreased as a consequence of increasing the temperature by 10°C. This effect too, is comparable to the general patterns of enzyme behavior in biological systems [80, 81]. Taken together, these observations also carry the implication that moderate, i.e., 50°C, and not high temperatures, were likely favorable to the catalytic reactions from the view of efficiency and speed of the catalyst.

In actuality, the catalytic activity of the nanoparticles remained high after removal from their source (IO) for days, even when stored at −18°C, demonstrated by a storage experiment (**Table 4**) [29], which further suggested that IO nanoparticles can be displaced to a considerable distance from their source and still

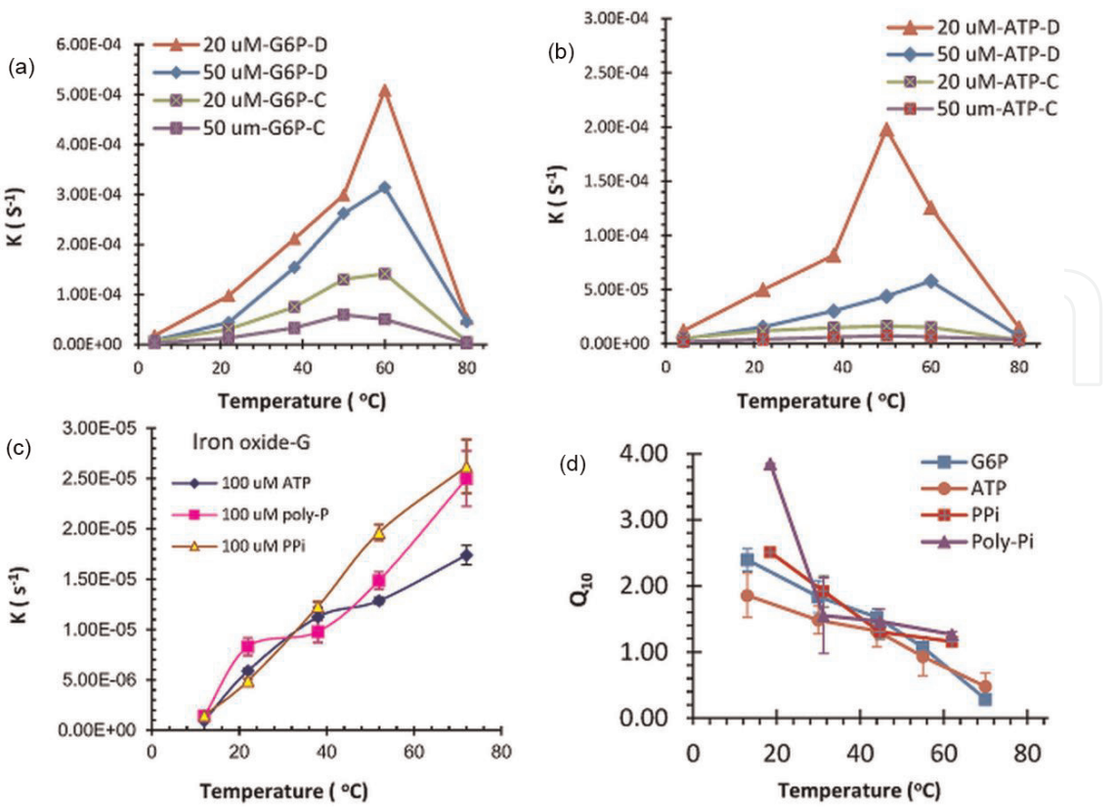

Figure 6.
*Relationship between environment temperature and the hydrolysis rate of phosphorus. (a) G6P, (b) ATP, (c) polyphosphate, and (d) the temperature coefficient Q_{10} (for details of IOs see **Table 1**).*

Treatment		20 μM G6P			20 μM ATP		
		1 h P_i (μM)	5 h P_i (μM)	$t_{0.5}$ (h)	1 h P_i (μM)	5 h P_i (μM)	$t_{0.5}$ (h)
11 days at 22°C	11R	5.49 ± 0.004	13.89 ± 0.064	3.2	4.47 ± 0.016	9.87 ± 0.255	6.0
11 days at 4°C	11 L	5.51 ± 0.010	13.64 ± 0.042	3.3	4.36 ± 0.005	9.71 ± 0.066	6.3
5 days frozen (−18°C) and 6 days at 4°C	5F6L	4.57 ± 0.013	11.48 ± 0.030	4.5	3.76 ± 0.009	7.61 ± 0.043	9.4
5 days at 4°C and 6 days at 22°C	5L6R	5.85 ± 0.011	14.10 ± 0.211	3.1	4.51 ± 0.018	10.30 ± 0.123	5.7
5 days at 50°C and 6 days at 22°C	5H6R	2.93 ± 0.01	6.68 ± 0.020	11	2.71 ± 0.012	4.92 ± 0.032	19
5 days at 50°C and 6 days at 4°C	5H6L	2.62 ± 0.002	5.44 ± 0.001	16	2.48 ± 0.002	3.72 ± 0.04	36
9 days at 50°C and 2 days at 22°C	9H2R	2.43 ± 0.005	4.07 ± 0.005	26	2.38 ± 0.016	3.08 ± 0.025	60

[a]*The P_i of the 20 μM G6P (DIW, control) after 120 h at the room temperature was changed from 1.67 to 1.83 μM. The corresponding half-life was 10,450 h. The P_i of the 20 μM ATP (DIW, control) after 120 h at the room temperature was changed from 1.89 to 2.07 μM. The corresponding half-life was 9290 h.*

Table 4.
Effect of storage conditions on the catalysis activity of iron oxide (IO-F) nanoparticle solutions.[a]

maintain catalytic activities for a considerable time. Meanwhile, low temperatures, even frozen conditions, also favor the persistence of catalytic activity from these IO nanoparticles. These are important from the view of astrobiology (origin of life) [28], but also for plant acquisition, nanoengineering and the potential application for industrial production.

6. Effect of pH and buffer solution

pH is another key factor for enzyme activity. The aged inorganic iron solution or the water bearing iron oxide nanoparticles, e.g., DMT-IO, are generally mildly acidic (pH 5.5–6.5). Various concentrations of bicarbonate were introduced in the DMT-IO system, but in all cases enzyme-like activity for phosphate ester hydrolysis remained quite high (**Figure 7a**). In general, the most favorable pH of the enzyme-like activity was found to be between 6 and 7, though the phosphorus source, the concentrations of bicarbonate, and the type of DMT-IO also influenced its activity (**Figure 7b** and **c**). When pH was raised beyond 7 (e.g., pH 7, 7.2 and 8), the catalysis coefficient, k, decreased as the concentration of HCO_3 increased, especially for the DMT-IO-D. When pH in solution was <7 (e.g., pH 6.2, 6.4, and 6.8), however, there were no clear patterns of k with respect to the concentration of HCO_3 and both the ATP and G6P in these two nanoparticles-bearing solutions. At the same time, k at weak acidic conditions (pH 6.2–6.8) was much higher than at weak base conditions (pH 7–8). This conclusion was further supported by an additional experiment involving the hydrolysis of ATP, whereby the pH values of DMT-IO solution were extended from 4 to 9.3 units by employing four different buffer systems (1.0 M acetate buffer (pH 4.0–5.6), 0.2 M dimethylglutaric acid buffer (pH 4.2–6.8), 20 mM $NaHCO_3$ (pH 7.6–9.3), and 40 mM $NaHCO_3$ (pH 5.8–9.3)) (**Figure 7d**).

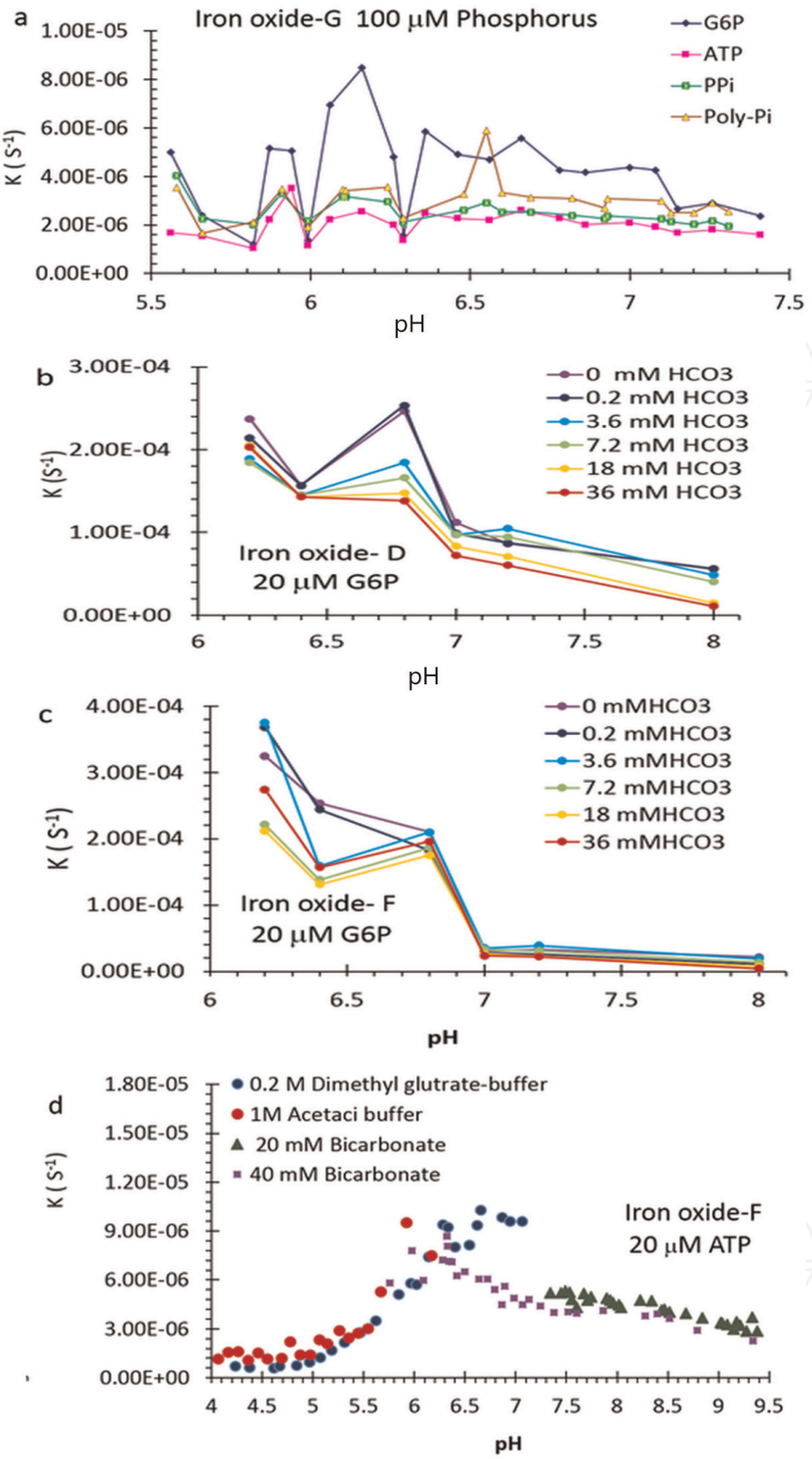

Figure 7.
Relationship between pH and the hydrolysis rate of phosphorus. (a) 100 μM four phosphorus in DMT-IO-G; (b) and (c) bicarbonate concentration on 20 μM G6P DMT-IO-D and F; (d) different buffers for 20 μM ATP in DMT-IO-F (for details of IOs see ***Table 1****).*

It should be pointed out that the catalysis capacity of these solutions bearing inorganic iron oxide nanoparticles is closely related to the buffer used in the system. The catalytic activity dropped precipitously after a small amount of citrate buffer (pH 4.0–6.2) or tris(hydroxymethyl)-aminomethane (TRIS) (pH 5.8–7.2) was introduced into an inorganic iron solution (**Table 5**). Both citrate [83, 84] and

Treatment[a]	Initial G6P (μM)	Reaction time (h)	P_i (μM)	Rate constant k (10^{-6} s^{-1})	Half-life $t_{0.5}$ (h)
DIW and aged 14 mo., 1000 nM, $Fe(NO_3)_3$, (1:1)	20	0	0.22	22.1	8.7
		1	1.75		
		2	3.37		
		6	7.74		
Aged 14 mo., $Fe(NO_3)_3$, 1000 nM and tris–HCl buffer (10 mM, pH 7.0), 1:1	20	0	0.22	1.72	111.8
		1	0.35		
		2	0.41		
		6	0.93		
DIW and aged 14 mo., 1000 nM, $Fe(NO_3)_3$, (1:1)	50	0	0.44	11.3	17.1
		1	2.45		
		2	4.58		
		6	11.14		
Aged 14 mo., $Fe(NO_3)_3$, 1000 nM and tris–HCl buffer (10 mM, pH 7.0), 1:1	50	0	0.44	1.93	99.8
		1	0.71		
		2	0.99		
		6	2.45		

[a]*Buffer experiments were conducted with a 1000 nM aged (14-month) inorganic iron solution. The iron solution diluted by DIW (1:1) was used as a control. Either 4 ml of 10 mM Tris-HCl (pH 7.0) or 4 ml of DIW was mixed with a 4 ml of aged iron solution, then 0.1 ml of 1.6 or 4.0 mM G6P stock solution was added to make a final solution containing 20 or 50 μM G6P. P_i concentration was determined at 0, 0.17, 1, 2 and 6 h, respectively, after the addition of G6P. The results of P_i in the table was an average of three replications. The rate constant and half-life were calculated based on the first order kinetics.*

Table 5.
Interaction between Tris-HCl buffer and aged inorganic iron solution on the hydrolysis rate of G6P.[a]

TRIS [85] can react with Fe (III) in solution to form the aqueous Fe-complex, particularly at high ratios of citrate or TRIS to Fe (>>10,000:1 molar ratio). But the catalysis of these solutions does not change when the acetic acid-acetate buffer system was introduced, the final acetate concentration in the solution was up to 0.25 M. All of these responses imply that the significant change was not due to the pH itself, but to the interactions between nanoparticles in the solution and chemicals in the environment. It has been reported that some buffer systems can significantly inhibit the activity of natural enzymes, for example, citrate on special PAPs [86] and alkaline phosphatase [87] and TRIS on aminopeptidase and RimO methylthiotransferase [88, 89] due to structure changes and metal-complex formation [84, 85, 90].

7. Natural and inorganic phosphatase

Recall the natural phosphatase, a binuclear metal center (di-iron Fe-Fe or Fe-M (M as Mn and Zn)) that produces orthophosphate due to the net transfer of the phosphoryl group to water, is essential for its catalysis (**Figure 8a**) [19, 66, 91–94]. The μ-(hydr)oxo ligand bridges in the metal center—the key of "phosphoesterase motif"—are a universal feature in binuclear phosphoesterase [19, 94]. They are responsible for the cleavage of phosphoester bonds; including acid and alkaline

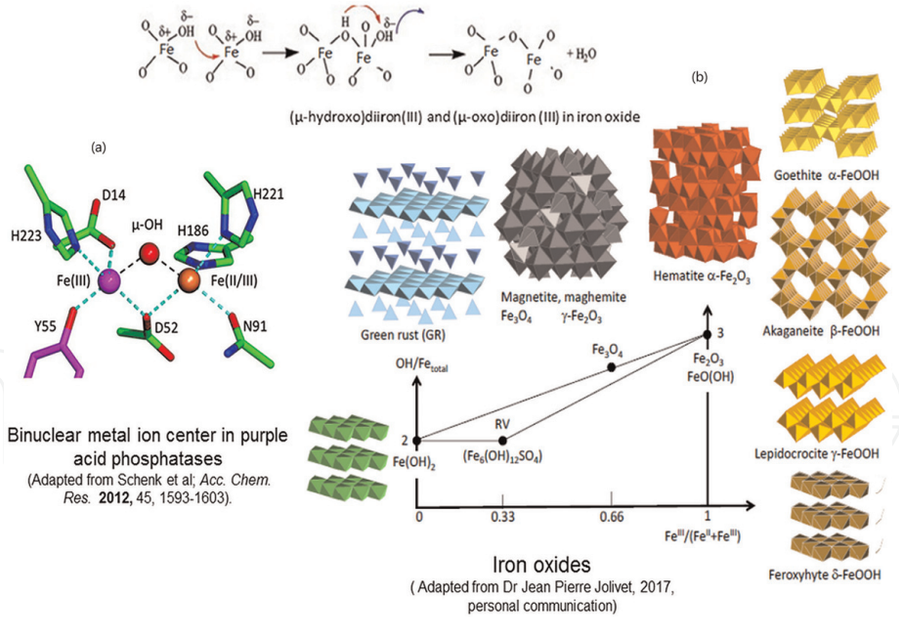

Figure 8.
The metal center of phosphatase. (a) The μ-(hydr)oxo-bridges in purple acid phosphatase (PAP), and (b) Fe-Fe structure in different iron oxides phases.

phosphatases; bacterial exonucleases; diadenosine tetraphosphatase; 5′-nucleotidase; phosphodiesterase; sphingomyelin phosphodiesterase, an enzyme involved in RNA debranching; and a phosphatase in the bacteriophage genome as well as for the family of Ser/Thr protein phosphatase (PP1, PP2A, and calcineurin) [95, 96]. Based on the μ-(hydr)oxo metal bridge structure, different artificial phosphatases have been synthesized by using different organic ligands to stabilize the metal center [19, 97, 98].

It is well known that iron speciation changes due to ion (III) hydrolysis in the solution during the aging process, diiron or polyirons oxide with the oxo-bridge or hydroxo-bridge (bond) might be formed [99–103]. Based on the quantum-chemical calculations by density-functional theory, dihydroxobridging binuclear compounds can be present in aqueous solutions, as binuclear dihydroxobridging $[Fe(H_2O)_4(\mu\text{-}OH)_2Fe(H_2O)_4]^{n+}$ and oxobridging $[Fe(H_2O)_5(\mu\text{-}O)Fe{\cdot}(H_2O)_5]^{n+}$ (n = 2, 4) cations in the hydrolysis products of cations $[Fe(H_2O)_6]^{m+}$ (m = 2, 3) [104]. The hydroxo-bridged Fe-$(OH)_2$-Fe dimers are the structure units in the polymetric hydroxo complex, which are dependent on pH and aging time [105, 106]. Molecular dynamics simulation further demonstrated the presence of aqueous di-iron or poly-irons, in which the Fe-Fe distance is 3.0–3.5 Å, with bonds by oxo-bridge or hydroxo-bridge [107]. Meanwhile, the (hydr)oxo-bridged Fe-Fe structure has been confirmed by experiments in the interface of iron oxide (IO, solid) to water [108–111]. The μ-oxo iron ion have been identified in-situ in the high concentrated inorganic iron solution (e.g., 0.1 M $Fe(NO_3)_3$ [101], and 0.1 M $FeCl_3$ [112]. The solubility of IOs further indicates that the critical ferrihydrite nucleus with an equivalent diameter of ~15 Å and containing only ~30 Fe atoms is stable in aqueous solution [113]. The 10-angstrom discrete iron-oxo cluster (known as the Keggin ion, Fe_{13}) is also soluble [114], as a constitute structure of ferrihydrite nanoparticles [102]. Consequently, iron oxide nanoparticles with 3.5 Å oxo-Fe bindings (e.g., doubly shared iron octahedra) such as ferrihydrite, goethite, hematite, magnetite, and even green rust (fougerite) can be presented in the natural environment (**Figure 8b**) [115–121]. Therefore, it is reasonable to suggest that the oxo bridged Fe-Fe structure in the aqueous IO nanoparticles contribute to the catalysis of phosphate ester hydrolysis [28]. This compares to the activity of the aged nanomolar inorganic iron ion solutions [26, 27] and mimics of the artificial phosphatases

[19, 97, 98]. The common feature between these IO nanoparticles, either from the DMT-IO or the aged inorganic iron ion solutions, as well as the natural or synthesized biomimetic phosphoesterase, constitute a kind of acceleration of electron transfer rate in the structure of the μ-(hydr)oxo ligand between the metals, particularly iron [19, 26–28, 92, 94, 122, 123]. In other words, the hydrolysis of phosphate ester is entirely dependent on its catalysis on this special Fe-oxo-Fe structure [27, 28]. Experiments and chemical models have also demonstrated that temperature impacts the stability of the aqueous poly-iron formation [124] and the nanostructure of IO in the solution [117, 125], which can explain the thermal denaturation behavior of the inorganic phosphatase (**Figure 6**). The Fe-Fe structure in the nanoparticles due to the nanosize-induced phase transformation and changes in the IO nanoparticle solution with the dissolved CO_2 [126] further supported the response of the inorganic phosphatase at different pH (**Figure 7**).

Similar to phosphatases, the active metal centers of most peroxidase and catalases in nature also comprise the transition metals, for example, horseradish peroxidase, HRP [127], heme catalases [128], uroerythrin [129] with Fe, manganese peroxidase [130], manganese catalases [131, 132] with Mn or haloperoxidases [133] with V, all exhibit the oxo ligand structure. This unique structure might be also accountable for the "intrinsic peroxidase or catalases" from different inorganic metal oxides nanoparticles [44, 48, 49, 51, 53, 54, 58–61, 134, 135]. It was noted that some PAPs were also reported to have activity of peroxidases [136, 137]. The K_m in **Table 3**, which denotes the affinities of the phosphate ester to catalysis, are significantly (up to three orders of magnitude) lower than that of natural PAPs [33, 66, 69, 91, 138, 139]. The same patterns were also observed for these inorganic peroxidases compared to its corresponding HRP [28]. This finding further indicates that the IO nanoparticles are either much more sensitive to the low concentration of phosphate ester or H_2O_2 in the environment, or they have a much higher affinity for phosphate esters or H_2O_2 compared to the natural enzymes, although the maximum velocity of the hydrolysis was relatively low with these IO nanoparticles, especially for high phosphate ester or H_2O_2 concentrations in the environment. Like the nanoparticles of IO and vanadium pentoxide, the intrinsic sulfite oxidase activity of molybdenum trioxide nanoparticles is also due to the oxo ligand of Mo, as revealed in the metal center of sulfite oxidase [62, 140, 141]. Essentially, the catalytic activities depend to some degree on the surface area of these nanoparticles, but not just merely on particle size [48, 51, 52, 134, 142, 143]. The in situ Raman spectroscopy on the changes of V-oxo (V=O) bond in the different V_2O_5 nanomaterials during H_2O_2 catalysis cycle further demonstrated that the catalytic characteristics in these nanoparticles is directly related to the metal structure in the nanoparticle surface [61], which supports the concept of inorganic enzyme [27, 28].

Several recently studies from Europe have suggested that iron-rich nanoparticles (<20 nm) are the main carriers of phosphorus in forest streams and soil solution [10, 11, 144, 145] and monoesters are the main composition of dissolved organic phosphorus in soil and water [10, 15, 16, 18]. This further imply that iron oxide nanoparticles might play a significantly role for the organic phosphorus transformation from the view of phosphorus biogeochemistry, although sorption and precipitation is still the dominant view of the current soil and environmental science on the interaction of iron oxides and dissolved organic phosphorus in soil and sediment [21, 146–149]. A couple of studies still noticed that orthophosphate can be released during the processing of the interactions [5, 20–25]. As iron oxide nanoparticles are very common and widely exist in the soil, sediment, dust, and water [125, 150–153], such enzyme-like catalytic propensities on phosphate esters in the current earth environment may provide an undiscovered feedback of organic phosphorus and play a critical role in the phosphorus cycles.

On the other hand, many effects have been made to improve inorganic nanozyme, both its catalysis capacity and substrate specificity, particularly for the "engineering peroxidase" related to iron oxide for its analytical, biomedical, and environmental applications from the view of nanoengineering [46, 47, 154, 155]. Various polymers or other organic compounds, e.g., porphyrin rings, the backbones of short peptides, amino acids, and even DNA, have been employed in the stabilization of the oxo bridged Fe-metal center in different iron oxides [156–160]. Similar effects should be made for the inorganic phosphatase as well. These "engineering phosphatase" can be employed for environmental monitors after standardization to assess the availability of dissolved organic phosphorus in waters and its potential risk for water eutrophication due to its higher stability and lower cost than protein enzymes, supported by the fact that natural phosphatase has been used for the tool to assess water or soil phosphorus availability [161–164]. Another possibility for industry is to use these high efficiencies engineered phosphatase to release the orthophosphate from the wastewater directly for agriculture.

8. Conclusions and future prospective

Laboratory experiments on the hydrolysis of phosphate ester in water demonstrated that inorganic phosphoesterase-like activity, using various inorganic iron oxide nanoparticles, significantly promotes the hydrolysis of phosphate ester, including G6P, PP_i, and ATP. These findings and the fact that this and other inorganic nanoparticles can act effectively as enzymes: for example, iron oxide as peroxidase, vanadium pentoxide as bromoperoxidase, and molybdenum trioxide nanoparticles as sulfite oxidase; further support the concept of inorganic enzymes. The catalytic property of these nanoparticles is likely due to the structure of the metal oxides or metal bonds in the oxides and not merely to the nanoparticle surfaces. As iron oxide nanoparticles are very common and widely exist in the soil, sediment, and water, such enzyme-like catalytic propensities on phosphate esters, the main composition of dissolved organic phosphorus, in the current earth environment may play a critical role in the phosphorus cycles.

Acknowledgements

This work is dedicated to my beloved parents (Dr. Jing-Xiong Ji and late Dr. Shi-Xiong Huang) and my family (Wei Sun and Jack Jixiang Huang) for their love, endless support, encouragement & sacrifices. X.L.H. greatly appreciates the precious comments from the late Dr. R.J.P. Williams in the past years, and the kindly permissions to use the structure of iron oxide (**Figure 8b**) from Dr. Jean Pierre Jolivet as well as the personal encouragements from Drs. Robert Atlas, Gerhard Schenk, Michael J. Russell, Jia-Zhong Zhang, Raghuraman Venkatapathy and Peter B. Ortner. The experiment part of this work was initially conducted by X.L H from 2007 to 2008 at the AOML, NOAA, supported by the National Oceanic and Atmospheric Administration's (NOAA) Coastal Ocean Program and Climate and Global Change Program. The research was carried out, in part, under the auspices of the Cooperative Institute of Marine and Atmospheric Studies (CIMAS), a joint institute of the University of Miami and NOAA, cooperative agreement #NA67RJ0149. The statements, findings, conclusions, and recommendations are those of the author and do not necessarily reflect the views of CIMAS, NOAA or the U.S. Department of Commerce.

Conflict of interest

The author declares no competing financial interest.

Author details

Xiao-Lan Huang
Independent Researcher, Cincinnati, OH, USA

*Address all correspondence to: xiaolan.huang@ymail.com

References

[1] Paytan A, McLaughlin K. The oceanic phosphorus cycle. Chemical Reviews. 2007;**107**:563-576. DOI: 10.1021/cr0503613

[2] Smil V. Phosphorus in the environment: Natural flows and human interferences. Annual Review of Energy and the Environment. 2000;**25**:53-88. DOI: 10.1146/annurev.energy.25.1.53

[3] Shen J, Yuan L, Zhang J, Li H, Bai Z, Chen X, et al. Phosphorus dynamics: From soil to plant. Plant Physiology. 2011;**156**:997-1005. DOI: 10.1104/pp.111.175232

[4] Reinhard CT, Planavsky NJ, Gill BC, Ozaki K, Robbins LJ, Lyons TW, et al. Evolution of the global phosphorus cycle. Nature. 2016;**541**:386. DOI: 10.1038/nature20772

[5] Baldwin DS. Organic phosphorus in the aquatic environment. Environmental Chemistry. 2013;**10**:439-454. DOI: 10.1071/EN13151

[6] Karl DM, Björkman KM. Chapter 5—Dynamics of dissolved organic phosphorus. In: Carlson CA, editor. Biogeochemistry of Marine Dissolved Organic Matter. 2nd ed. Boston: Academic Press; 2015. pp. 233-334. DOI: 10.1016/B978-0-12-405940-5.00005-4

[7] Huang L-M, Jia X-X, Zhang G-L, Shao M-A. Soil organic phosphorus transformation during ecosystem development: A review. Plant and Soil. 2017;**417**:17-42. DOI: 10.1007/s11104-017-3240-y

[8] Dodd RJ, Sharpley AN. Recognizing the role of soil organic phosphorus in soil fertility and water quality. Resources, Conservation and Recycling. 2015;**105**:282-293. DOI: 10.1016/j.resconrec.2015.10.001

[9] McLaren TI, Smernik RJ, McLaughlin MJ, McBeath TM, Kirby JK, Simpson RJ, et al. Complex forms of soil organic phosphorus—A major component of soil phosphorus. Environmental Science & Technology. 2015;**49**:13238-13245. DOI: 10.1021/acs.est.5b02948

[10] Jiang X, Bol R, Cade-Menun BJ, Nischwitz V, Willbold S, Bauke SL, et al. Colloid-bound and dissolved phosphorus species in topsoil water extracts along a grassland transect from Cambisol to Stagnosol. Biogeosciences. 2017;**14**:1153-1164. DOI: 10.5194/bg-14-1153-2017

[11] Missong A, Holzmann S, Bol R, Nischwitz V, Puhlmann H, Wilpert K, et al. Leaching of natural colloids from forest topsoils and their relevance for phosphorus mobility. Science of the Total Environment. 2018;**634**:305-315. DOI: 10.1016/j.scitotenv.2018.03.265

[12] Wang Z-H, Liang Y, Kang W. Utilization of dissolved organic phosphorus by different groups of phytoplankton taxa. Harmful Algae. 2011;**12**:113-118. DOI: 10.1016/j.hal.2011.09.005

[13] Ged EC, Boyer TH. Molecular weight distribution of phosphorus fraction of aquatic dissolved organic matter. Chemosphere. 2013;**91**:921-927. DOI: 10.1016/j.chemosphere.2013.01.113

[14] Ni Z, Wang S, Wang Y. Characteristics of bioavailable organic phosphorus in sediment and its contribution to lake eutrophication in China. Environmental Pollution. 2016;**219**:537-544. DOI: 10.1016/j.envpol.2016.05.087

[15] Bell Douglas W, Pellechia P, Chambers LR, Longo Amelia F, McCabe Kelly M, Ingall Ellery D, et al. Isolation

and molecular characterization of dissolved organic phosphorus using electrodialysis-reverse osmosis and solution 31P-NMR. Limnology and Oceanography: Methods. 2017;**15**: 436-452. DOI: 10.1002/lom3.10171

[16] Duhamel S, Björkman KM, Repeta DJ, Karl DM. Phosphorus dynamics in biogeochemically distinct regions of the southeast subtropical Pacific Ocean. Progress in Oceanography. 2017;**151**: 261-274. DOI: 10.1016/j.pocean.2016.12.007

[17] Liu S, Zhu Y, Wu F, Meng W, Wang H, He Z, et al. Using solid 13C NMR coupled with solution 31P NMR spectroscopy to investigate molecular species and lability of organic carbon and phosphorus from aquatic plants in Tai Lake, China. Environmental Science and Pollution Research. 2017;**24**: 1880-1889. DOI: 10.1007/s11356-016-7954-9

[18] Menezes-Blackburn D, Giles C, Darch T, George TS, Blackwell M, Stutter M, et al. Opportunities for mobilizing recalcitrant phosphorus from agricultural soils: A review. Plant and Soil. 2018;**427**:5-16. DOI: 10.1007/s11104-017-3362-2

[19] Schenk G, Mitić N, Hanson GR, Comba P. Purple acid phosphatase: A journey into the function and mechanism of a colorful enzyme. Coordination Chemistry Reviews. 2013; **257**:473-482. DOI: 10.1016/j.ccr.2012.03.020

[20] Baldwin DS, Beattie JK, Coleman LM, Jones DR. Phosphate ester hydrolysis facilitated by mineral phases. Environmental Science and Technology. 1995;**29**:1706-1709. DOI: 10.1021/es00006a040

[21] Huang X-L, Zhang J-Z. Spatial variation in sediment-water exchange of phosphorus in Florida bay: AMP As a model organic compound. Environmental Science & Technology. 2010;**44**:7790-7795. DOI: 10.1021/es100057r

[22] Olsson R, Giesler R, Loring JS, Persson P. Adsorption, desorption, and surface-promoted hydrolysis of glucose-1-phosphate in aqueous goethite (α-FeOOH) suspensions. Langmuir. 2010;**26**:18760-18770. DOI: 10.1021/la1026152

[23] Persson P, Andersson T, Nelson H, Sjöberg S, Giesler R, Lövgren L. Surface complexes of monomethyl phosphate stabilized by hydrogen bonding on goethite (α-FeOOH) nanoparticles. Journal of Colloid and Interface Science. 2012;**386**:350-358. DOI: 10.1016/j.jcis.2012.07.042

[24] Mäkie P, Westin G, Persson P, Österlund L. Adsorption of trimethyl phosphate on maghemite, hematite, and goethite nanoparticles. The Journal of Physical Chemistry A. 2011;**115**: 8948-8959. DOI: 10.1021/jp201065w

[25] Lü C, Yan D, He J, Zhou B, Li L, Zheng Q. Environmental geochemistry significance of organic phosphorus: An insight from its adsorption on iron oxides. Applied Geochemistry. 2017;**84**: 52-60. DOI: 10.1016/j.apgeochem.2017.05.026

[26] Huang XL, Zhang JZ. Sediment-Water Exchange of Dissolved Organic Phosphorus in Florida Bay. Miami, FL: Cooperative Institute for Marine and Atmospheric Studies; 2007

[27] Huang XL, Zhang JZ. Hydrolysis of glucose-6-phosphate in aged, acid-forced hydrolysed nanomolar inorganic iron solutions—An inorganic biocatalyst? RSC Advances. 2012;**2**: 199-208. DOI: 10.1039/C1RA00353D

[28] Huang XL. Hydrolysis of phosphate esters catalyzed by inorganic iron oxide nanoparticles acting as biocatalysts.

Astrobiology. 2018;**18**:294-310. DOI: 10.1089/ast.2016.1628

[29] Bunton CA, Chaimovich H. The acid-catalyzed hydrolysis of pyrophosphoric acid. Inorganic Chemistry. 1965;**4**:1763-1766

[30] Sigel H, Amsler PE. Hydrolysis of nucleoside phosphates. 6. On the mechanism of the metal ion promoted dephosphorylation of purine nucleoside 5′-triphosphates. Journal of the American Chemical Society. 1976;**98**: 7390-7400

[31] Milburn RM, Gautem-Basek M, Tribolet R, Sigel H. Comparison of the effectiveness of various metal ions on the promoted dephosphorylation of adenosine 5′-triphosphate (ATP) and uridine 5′-triphosphate (UTP)2. Journal of the American Chemical Society. 1985; **107**:3315-3321

[32] Sigel H. Mechanistic aspects of the metal ion promoted hydrolysis of nucleoside 5′-triphosphates (NTPs). Coordination Chemistry Reviews. 1990; **100**:453-539

[33] Schenk G, Ge Y, Carrington LE, Wynne CJ, Searle IR, Carroll BJ, et al. Binuclear metal centers in plant purple acid phosphatases: Fe-Zn in sweet potato and Fe-Zn in soybean. Archives of Biochemistry and Biophysics. 1999;**370**:183-189. DOI: 10.1006/abbi.1999.1407

[34] Blasko A, Bruice TC. Recent studies of nucleophilic, general-acid, and metal ion catalysis of phosphate diester hydrolysis. Accounts of Chemical Research. 1999;**32**:475-484. DOI: 10.1021/ar980060y

[35] Liu C, Yu S, Li D, Liao Z, Sun X, Xu H. DNA hydrolytic cleavage by the diiron(III) complex Fe(DTPB)(μ-O)(μ-Ac)Cl(BF): Comparison with other binuclear transition metal complexes. Inorganic Chemistry. 2002;**41**:913-922. DOI: 10.1021/ic010302h

[36] Karsten P, Neves A, Bortoluzzi AJ, Lanznaster M, Drago V. Synthesis, structure, properties, and phosphatase-like activity of the first heterodinuclear FeMn complex with the unsymmetric ligand HBPBPMP as a model for the PAP in sweet potato. Inorganic Chemistry. 2002;**41**:4624-4626. DOI: 10.1021/ic025674k

[37] Atkinson RJ. Adsorption of potential-determining ions at the ferric oxide-aqueous electrolyte interface. Journal of Physical Chemistry. 1967;**71**: 550-558

[38] Schwertmann U, Cornell RM. Iron Oxides in the Laboratory: Preparation and Characterization. Weinheim, New York, Chichester Brisbane, Singapore, Toronto: WILEY-VCH Verlag GmbH; 2007

[39] Zhang J-Z, Kelble C, Millero FJ. Gas-segmented continuous flow analysis of iron in water with a long liquid waveguide capillary flow cell. Analytica Chimica Acta. 2001;**438**:49-57. DOI: 10.1016/S0003-2670(01)01031-5

[40] Sigel H. Have adenosine 5′-triphosphate ATP4- and related purine-nucleotides played a role in early evolution? ATP, its own 'enzyme' in metal ion facilitated hydrolysis! Inorganica Chimica Acta. 1992;**198-200**: 1-11

[41] Torrents A, Stone AT. Hydrolysis of phenyl picolinate at the mineral/water interface. Envirenmental Science and Technology. 1991;**25**:143-149

[42] Baldwin DS, Beattie JK, Coleman LM, Jones DR. Hydrolysis of an organophosphate ester by manganese dioxide. Environmental Science and Technology. 2001;**35**:713-716. DOI: 10.1021/es001309l

[43] Bardsley WG, Leff P, Kavanagh J, Waight RD. Deviations from Michaelis-Menten kinetics. The possibility of complicated curves for simple kinetic schemes and the computer fitting of experimental data for acetylcholinesterase, acid phosphatase, adenosine deaminase, arylsulphatase, benzylamine oxidase, chymotrypsin, fumarase, galactose dehydrogenase, beta-galactosidase, lactate dehydrogenase, peroxidase and xanthine oxidase. Biochemical Journal. 1980;**187**:739-765

[44] Gao L, Zhuang J, Nie L, Zhang J, Zhang Y, Gu N, et al. Intrinsic peroxidase-like activity of ferromagnetic nanoparticles. Nature Nanotechnology. 2007;**2**:577-583. DOI: 10.1038/nnano.2007.260

[45] Lin Y, Ren J, Qu X. Catalytically active nanomaterials: A promising candidate for artificial enzymes. Accounts of Chemical Research. 2014; **47**:1097-1105. DOI: 10.1021/ar400250z

[46] Gao L, Fan K, Yan X. Iron oxide nanozyme: A multifunctional enzyme mimetic for biomedical applications. Theranostics. 2017;**7**:3207-3227. DOI: 10.7150/thno.19738

[47] Karsten K, Nawaz TM, Wolfgang T. A step into the future: Applications of nanoparticle enzyme mimics. Chemistry-A European Journal. 2018; **24**:9703-9713. DOI: 10.1002/ chem.201800384

[48] Chaudhari KN, Chaudhari NK, Yu JS. Peroxidase mimic activity of hematite iron oxides (α-Fe_2O_3) with different nanostructures. Catalysis Science and Technology. 2012;**2**: 119-124. DOI: 10.1039/c1cy00124h

[49] Chen Z, Yin JJ, Zhou YT, Zhang Y, Song L, Song M, et al. Dual enzyme-like activities of iron oxide nanoparticles and their implication for diminishing cytotoxicity. ACS Nano. 2012;**6**: 4001-4012. DOI: 10.1021/nn300291r

[50] Peng C, Jiang B, Liu Q, Guo Z, Xu Z, Huang Q, et al. Graphene-templated formation of two-dimensional lepidocrocite nanostructures for high-efficiency catalytic degradation of phenols. Energy and Environmental Science. 2011;**4**:2035-2040. DOI: 10.1039/c0ee00495b

[51] Mu J, Zhang L, Zhao G, Wang Y. The crystal plane effect on the peroxidase-like catalytic properties of Co_3O_4 nanomaterials. Physical Chemistry Chemical Physics. 2014;**16**: 15709-15716. DOI: 10.1039/c4cp01326c

[52] Peng Y, Wang Z, Liu W, Zhang H, Zuo W, Tang H, et al. Size- and shape-dependent peroxidase-like catalytic activity of $MnFe_2O_4$ nanoparticles and their applications in highly efficient colorimetric detection of target cancer cells. Dalton Transactions. 2015;**44**: 12871-12877. DOI: 10.1039/C5DT01585E

[53] Vernekar AA, Das T, Ghosh S, Mugesh G. A remarkably efficient $MnFe_2O_4$-based oxidase nanozyme. Chemistry—An Asian Journal. 2016;**11**: 72-76. DOI: 10.1002/asia.201500942

[54] Su L, Qin W, Zhang H, Rahman ZU, Ren C, Ma S, et al. The peroxidase/catalase-like activities of MFe_2O_4 (M = Mg, Ni, Cu) MNPs and their application in colorimetric biosensing of glucose. Biosensors and Bioelectronics. 2015;**63**:384-391. DOI: 10.1016/j.bios.2014.07.048

[55] Su L, Feng J, Zhou X, Ren C, Li H, Chen X. Colorimetric detection of urine glucose based $ZnFe_2O_4$ magnetic nanoparticles. Analytical Chemistry. 2012;**84**:5753-5758. DOI: 10.1021/ ac300939z

[56] Ray C, Dutta S, Sarkar S, Sahoo R, Roy A, Pal T. Intrinsic peroxidase-like activity of mesoporous nickel oxide for

selective cysteine sensing. Journal of Materials Chemistry B. 2014;**2**: 6097-6105. DOI: 10.1039/C4TB00968A

[57] Yang H, Xiong Y, Zhang P, Su L, Ye F. Colorimetric detection of mercury ions using MnO_2 nanorods as enzyme mimics. Analytical Methods. 2015;**7**: 4596-4601. DOI: 10.1039/c5ay00633c

[58] André R, Natálio F, Humanes M, Leppin J, Heinze K, Wever R, et al. V_2O_5 nanowires with an intrinsic peroxidase-like activity. Advanced Functional Materials. 2011;**21**:501-509. DOI: 10.1002/adfm.201001302

[59] Natalio F, André R, Hartog AF, Stoll B, Jochum KP, Wever R, et al. Vanadium pentoxide nanoparticles mimic vanadium haloperoxidases and thwart biofilm formation. Nature Nanotechnology. 2012;**7**:530-535. DOI: 10.1038/nnano. 2012.91

[60] Vernekar AA, Sinha D, Srivastava S, Paramasivam PU, D'Silva P, Mugesh G. An antioxidant nanozyme that uncovers the cytoprotective potential of vanadia nanowires. Nature Communications. 2014;**5**. Article ID: 5301. DOI: 10.1038/ncomms 6301

[61] Sourav G, Punarbasu R, Naiwrit K, Jemmis ED, Govindasamy M. Nanoisozymes: Crystal-facet-dependent enzyme-mimetic activity of V_2O_5 nanomaterials. Angewandte Chemie International Edition. 2018;**57**: 4510-4515. DOI: 10.1002/anie.2018 00681

[62] Ragg R, Natalio F, Tahir MN, Janssen H, Kashyap A, Strand D, et al. Molybdenum trioxide nanoparticles with intrinsic sulfite oxidase activity. ACS Nano. 2014;**8**:5182-5189. DOI: 10.1021/nn501235j

[63] Burman S, Davis JC, Weber MJ, Averill BA. The interaction of phosphate with the purple acid phosphatase from beef spleen: Evidence that phosphate binding is accompanied by oxidation of the iron chromophore. Biochemical and Biophysical Research Communications. 1986;**136**:490-497

[64] Pyrz JW, Sage JT, Debrunner PG, Que L Jr. The interaction of phosphate with uteroferrin. Characterization of a reduced uteroferrin-phosphate complex. Journal of Biological Chemistry. 1986;**261**: 11015-11020

[65] David SS, Que L Jr. Anion binding to uteroferrin. Evidence for phosphate coordination to the iron(III) ion of the dinuclear active site and interaction with the hydroxo bridge. Journal of the American Chemical Society. 1990;**112**: 6455-6463

[66] Vincent JB, Crowder MW, Averill BA. Spectroscopic and kinetics studies of a high-salt-stabilized form of the purple acid phosphatase from bovine spleen. Biochemistry. 1991;**30**: 3025-3034

[67] Crans DC, Simone CM, Holz RC, Que L Jr. Interaction of porcine uterine fluid purple acid phosphatase with vanadate and vanadyl cation. Biochemistry. 1992;**31**:11731-11739

[68] Schenk G, Carrington LE, Hamilton SE, Jersey JD, Guddat LW. Crystallization and preliminary X-ray diffraction data for a purple acid phosphatase from sweet potato. Acta Crystallographica Section D: Structural Biology. 1999;**55**:2051-2052. DOI: 10.1107/S0907444999012597

[69] Schenk G, Gahan LR, Carrington LE, Mitić N, Valizadeh M, Hamilton SE, et al. Phosphate forms an unusual tripodal complex with the Fe-Mn center of sweet potato purple acid phosphatase. Proceedings of the National Academy of Sciences of the United States of America. 2005;**102**:273-278. DOI: 10.1073/pnas.0407239102

[70] Wang Z, Ming LJ, Que L Jr, Vincent JB, Crowder MW, Averill BA. 1H NMR and NOE studies of the purple acid phosphatases from porcine uterus and bovine spleen. Biochemistry. 1992;**31**: 5263-5268

[71] Lim JS, Aquino MAS, Sykes AG. Mechanistic studies on the reactions of molybdenum(VI), tungsten(VI), vanadium(V), and arsenic(V) tetraoxo anions with the $Fe^{II}Fe^{III}$ form of purple acid phosphatase from porcine uteri (uteroferrin). Inorganic Chemistry. 1996;**35**:614-618. DOI: 10.1021/ic950139o

[72] Elliott TW, Mitić N, Gahan LR, Guddat LW, Schenk G. Inhibition studies of purple acid phosphatases: Implications for the catalytic mechanism. Journal of the Brazilian Chemical Society. 2006;**17**:1558-1565. DOI: 10.1590/S0103-50532006000800011

[73] Ferreira CV, Taga EM, Aoyama H. Glycolytic intermediates as substrates of soybean acid phosphatase isoforms. Plant Science. 1999;**147**: 49-54. DOI: 10.1016/S0168-9452(99)00096-5

[74] Wang X, Que L Jr. Extended X-ray absorption fine structure studies of the anion complexes of FeZn uteroferrin. Biochemistry. 1998;**37**:7813-7821. DOI: 10.1021/bi980150a

[75] Dietrich M, Munstermann D, Suerbaum H, Witzel H. Purple acid phosphatase from bovine spleen. Interactions at the active site in relation to the reaction mechanism. European Journal of Biochemistry. 1991;**199**: 105-113

[76] Crowder MW, Vincent JB, Averill BA. Electron paramagnetic resonance studies on the high-salt form of bovine spleen purple acid phosphatase. Biochemistry. 1992;**31**:9603-9608. DOI: 10.1021/bi00155a012

[77] Reiter NJ, White DJ, Rusnak F. Inhibition of bacteriophage g protein phosphatase by organic and oxoanion inhibitors. Biochemistry. 2002;**41**: 1051-1059. DOI: 10.1021/bi011577b

[78] Balogh E, Todea AM, Muller A, Casey WH. Rates of ligand exchange between $>Fe^{III}\text{-}OH_2$ functional groups on a nanometer-sized aqueous cluster and bulk solution. Inorganic Chemistry. 2007;**46**:7087-7092. DOI: 10.1021/ic7009308

[79] Elias M, Wieczorek G, Rosenne S, Tawfik DS. The universality of enzymatic rate-temperature dependency. Trends in Biochemical Sciences. 2014;**39**:1-7. DOI: 10.1016/j.tibs.2013.11.001

[80] Hobbs JK, Jiao W, Easter AD, Parker EJ, Schipper LA, Arcus VL. Change in heat capacity for enzyme catalysis determines temperature dependence of enzyme catalyzed rates. ACS Chemical Biology. 2013;**8**: 2388-2393. DOI: 10.1021/cb4005029

[81] Schipper LA, Hobbs JK, Rutledge S, Arcus VL. Thermodynamic theory explains the temperature optima of soil microbial processes and high Q10 values at low temperatures. Global Change Biology. 2014;**20**:3578-3586. DOI: 10.1111/gcb.12596

[82] Arcus VL, Prentice EJ, Hobbs JK, Mulholland AJ, Van der Kamp MW, Pudney CR, et al. On the temperature dependence of enzyme-catalyzed rates. Biochemistry. 2016;**55**:1681-1688. DOI: 10.1021/acs.biochem.5b01094

[83] Spiro TG, Bates G, Saltman P. The hydrolytic polymerization of ferric citrate. II. The influence of excess citrate. Journal of the American Chemical Society. 1967;**89**:5559-5562

[84] Silva AM, Kong X, Parkin MC, Cammack R, Hider RC. Iron(iii) citrate speciation in aqueous solution. Dalton

Transactions. 2009;**40**:8616-8625. DOI: 10.1039/B910970F

[85] Gupta BS, Taha M, Lee MJ. Stability constants for the equilibrium models of iron(III) with several biological buffers in aqueous solutions. Journal of Solution Chemistry. 2013;**42**:2296-2309. DOI: 10.1007/s10953-013-0107-6

[86] Nuttleman PR, Roberts RM. Transfer of iron from uteroferrin (purple acid phosphatase) to transferrin related to acid phosphatase activity. Journal of Biological Chemistry. 1990; **265**:12192-12199

[87] Evered DF, Steenson TI. Citrate inhibition of alkaline phosphatase. Nature. 1964;**202**:491-492

[88] Desmarais WT, Bienvenue DL, Bzymek KP, Holz RC, Petsko GA, Ringe D. The 1.20 Å resolution crystal structure of the aminopeptidase from *Aeromonas proteolytica* complexed with tris: A tale of buffer inhibition. Structure. 2002;**10**:1063-1072. DOI: 10.1016/S0969-2126(02)00810-9

[89] Molle T, Clémancey M, Latour J-M, Kathirvelu V, Sicoli G, Forouhar F, et al. Unanticipated coordination of tris buffer to the radical SAM cluster of the Rim O methylthiotransferase. JBIC Journal of Biological Inorganic Chemistry. 2016;**21**:549-557. DOI: 10.1007/s00775-016-1365-8

[90] Palmer DA, Drummond SE. Potentiometric determination of the molal formation constants of ferrous acetate complexes in aqueous solutions to high temperatures. Journal of Physical Chemistry. 1988;**92**:6795-6800

[91] LeBansky BR, McKnight TD, Gritting LR. Purification and characterization of a secreted purple phosphatase from soybean suspension cultures. Plant Physiology. 1992;**99**: 391-395. DOI: 10.1104/pp.99.2.391

[92] Sträter N, Lipscomb WN. Two-metal ion catalysis in enzymatic acyl- and phosphoryl-transfer reactions. Angewandte Chemie International Edition. 1996;**35**:2024-2055. DOI: 10.1002/anie.199620241

[93] Lindqvist Y, Johansson E, Kaija H, Vihko P, Schneider G. Three-dimensional structure of a mammalian purple acid phosphatase at 2.2 Å resolution with a μ-(hydr)oxo bridged di-iron center. Journal of Molecular Biology. 1999;**291**:135-147. DOI: 10.1006/jmbi.1999.2962

[94] Mitić N, Smith SJ, Neves A, Guddat LW, Gahan LR, Schenk G. The catalytic mechanisms of binuclear metallohydrolases. Chemical Reviews. 2006;**106**:3338-3363. DOI: 10.1021/cr050318f

[95] Lohse DL, Denu JM, Dixon JE. Insights derived from the structures of the Ser/Thr phosphatases calcineurin and protein phosphatase 1. Structure. 1995;**3**:987-990. DOI: 10.1016/S0969-2126(01)00234-9

[96] Rusnak F, Mertz P. Calcineurin: Form and function. Physiological Reviews. 2000;**80**:1483-1521. DOI: 10.1152/physrev.2000.80.4.1483

[97] Than R, Feldmann AA, Krebs B. Structural and functional studies on model compounds of purple acid phosphatases and catechol oxidases. Coordination Chemistry Reviews. 1999; **182**:211-241. DOI: 10.1016/S0010-8545(98)00234-3

[98] Belle C, Pierre JL. Asymmetry in bridged binuclear metalloenzymes: Lessons for the chemist. European Journal of Inorganic Chemistry. 2003;**23**:4137-4146. DOI: 10.1002/ejic.200300231

[99] Schwertmann U, Friedl J, Stanjek H. From Fe(III) ions to ferrihydrite and then to hematite. Journal of Colloid and

Interface Science. 1999;**209**:215-223. DOI: 10.1006/jcis.1998.5899

[100] Fu D, Keech PG, Sun X, Wren JC. Iron oxyhydroxide nanoparticles formed by forced hydrolysis: Dependence of phase composition on solution concentration. Physical Chemistry Chemical Physics. 2011;**13**: 18523-18529. DOI: 10.1039/C1CP20188C

[101] Zhu M, Puls BW, Frandsen C, Kubicki JD, Zhang H, Waychunas GA. In situ structural characterization of ferric iron dimers in aqueous solutions: Identification of μ-oxo species. Inorganic Chemistry. 2013;**52**: 6788-6797. DOI: 10.1021/ic302053w

[102] Weatherill JS, Morris K, Bots P, Stawski TM, Janssen A, Abrahamsen L, et al. Ferrihydrite formation: The role of Fe13 Keggin clusters. Environmental Science and Technology. 2016;**50**: 9333-9342. DOI: 10.1021/acs.est.6b02481

[103] Das B. Theoretical study of small iron-oxyhydroxide clusters and formation of ferrihydrite. Journal of Physical Chemistry A. 2018;**122**:652-661. DOI: 10.1021/acs.jpca.7b09470

[104] Panina N, Belyaev A, Eremin A, Davidovich P. DFT quantum-chemical study of the hydrolysis products of Fe (II) and Fe(III) aqua-complexes. Russian Journal of General Chemistry. 2010;**80**:889-894. DOI: 10.1134/s1070363210050038

[105] Pykhteev OY, Efimov AA. Hydrolytic polymerization of iron(III) in partially neutralized nitrate solutions. Russian Journal of Inorganic Chemistry. 1999;**44**:494-499

[106] Baev A, Evsei E. Distribution and reaction dynamics of iron(III) hydrolytic cationic species. Russian Journal of Inorganic Chemistry. 2010;**55**: 508-522. DOI: 10.1134/s00360236 10040054

[107] Zhang H, Waychunas GA, Banfield JF. Molecular dynamics simulation study of the early stages of nucleation of iron oxyhydroxide nanoparticles in aqueous solutions. Journal of Physical Chemistry B. 2015;**119**: 10630-10642. DOI: 10.1021/acs.jpcb.5b03801

[108] Barron V, Torrent J. Surface hydroxyl configuration of various crystal faces of hematite and goethite. Journal of Colloid and Interface Science. 1996;**177**:407-410. DOI: 10.1006/jcis.1996.0051

[109] Eggleston CM, Stack AG, Rosso KM, Higgins SR, Bice AM, Boese SW, et al. The structure of hematite (a-Fe_2O_3) (001) surfaces in aqueous media: Scanning tunneling microscopy and resonant tunneling calculations of coexisting O and Fe terminations. Geochimica et Cosmochimica Acta. 2003;**67**:985-1000. DOI: 10.1016/S0016-7037(02)01200-0

[110] Trainor TP, Chaka AM, Eng PJ, Newville M, Waychunas GA, Catalano JG, et al. Structure and reactivity of the hydrated hematite (0001) surface. Surface Science. 2004;**573**:204-224. DOI: 10.1016/j.susc.2004.09.040

[111] Tanwar KS, Lo CS, Eng PJ, Catalano JG, Walko DA, Brown GE Jr, et al. Surface diffraction study of the hydrated hematite surface. Surface Science. 2007;**601**:460-474. DOI: 10.1016/j.susc.2006.10.021

[112] Hellman H, Laitinen RS, Kaila L, Jalonen J, Hietapelto V, Jokela J, et al. Identification of hydrolysis products of $FeCl_3$ $6H_2O$ by ESI-MS. Journal of Mass Spectrometry. 2006;**41**:1421-1429. DOI: 10.1002/jms.1107

[113] Hiemstra T. Formation, stability, and solubility of metal oxide nanoparticles: Surface entropy, enthalpy, and free energy of ferrihydrite. Geochimica et Cosmochimica Acta.

2015;**158**:79-198. DOI: 10.1016/j.gca.2015.02.032

[114] Sadeghi O, Zakharov LN, Nyman M. Aqueous formation and manipulation of the iron-oxo Keggin ion. Science. 2015;**347**:1359-1362. DOI: 10.1126/science.aaa4620

[115] Rose J, Manceau A, Masion A, Bottero JY. Structure and mechanisms of formation of FeOOH(NO_3) oligomers in the early stages of hydrolysis. Langmuir. 1997;**13**:3240-3246. DOI: 10.1021/la962079k

[116] Jolivet JP, Tronc E, Chanéac C. Iron oxides: From molecular clusters to solid. A nice example of chemical versatility. Comptes Rendus-Geoscience. 2006;**338**: 488-497. DOI: 10.1016/j.crte.2006.04.014

[117] Navrotsky A, Mazeina L, Majzlan J. Size-driven structural and thermodynamic complexity in iron oxides. Science. 2008;**319**:1635-1638. DOI: 10.1126/science.1148614

[118] Zegeye A, Bonneville S, Benning LG, Sturm A, Fowle DA, Jones C, et al. Green rust formation controls nutrient availability in a ferruginous water column. Geology. 2012;**40**:599-602. DOI: 10.1130/G32959.1

[119] Michel FM, Ehm L, Antao SM, Lee PL, Chupas PJ, Liu G, et al. The structure of ferrihydrite, a nanocrystalline material. Science. 2007;**316**:1726-1729. DOI: 10.1126/science.1142525

[120] Michel FM, Barrón V, Torrent J, Morales MP, Serna CJ, Boily JF, et al. Ordered ferrimagnetic form of ferrihydrite reveals links among structure, composition, and magnetism. Proceedings of the National Academy of Sciences of the United States of America. 2010;**107**:2787-2792. DOI: 10.1073/pnas.0910170107

[121] Baumgartner J, Faivre D. Iron solubility, colloids and their impact on iron (oxyhydr)oxide formation from solution. Earth-Science Reviews. 2015; **150**:520-530. DOI: 10.1016/j.earscirev.2015.09.003

[122] Lassila JK, Zalatan JG, Herschlag D. Biological phosphoryl-transfer reactions: Understanding mechanism and catalysis. Annual Review of Biochemistry. 2011;**80**:669-702. DOI: 10.1146/annurev-biochem-060409-092741

[123] Duval S, Danyal K, Shaw S, Lytle AK, Dean DR, Hoffman BM, et al. Electron transfer precedes ATP hydrolysis during nitrogenase catalysis. Proceedings of the National Academy of Sciences of the United States of America. 2013;**110**:16414-16419. DOI: 10.1073/pnas.1311218110

[124] Milburn RM, Vosburgh WC. A spectrophotometric study of the hydrolysis of iron (III) ion, II. Polynuclear species. Journal of the American Chemical Society. 1955;**77**: 1352-1355

[125] Guo H, Barnard AS. Naturally occurring iron oxide nanoparticles: Morphology, surface chemistry and environmental stability. Journal of Materials Chemistry A. 2013;**1**:27-42. DOI: 10.1039/C2TA00523A

[126] Chernyshova IV, Ponnurangam S, Somasundaran P. Linking interfacial chemistry of CO_2 to surface structures of hydrated metal oxide nanoparticles: Hematite. Physical Chemistry Chemical Physics. 2013;**15**:6953-6964. DOI: 10.1039/c3cp44264k

[127] Gajhede M, Schuller DJ, Henriksen A, Smith AT, Poulos TL. Crystal structure of horseradish peroxidase C at 215 Å resolution. Nature Structural Biology. 1997;**4**:1032-1038

[128] Bravo J, Verdaguer N, Tormo J, Betzel C, Switala J, Loewen PC, et al.

Crystal structure of catalase HPII from *Escherichia coli*. Structure. 1995;**3**: 491-502. DOI: 10.1016/S0969-2126(01) 00182-4

[129] LeGall J, Prickril BC, Moura I, Xavier AV, Moura JJG, Huynh BH. Isolation and characterization of rubrerythrin, a non-heme iron protein from *Desulfovibrio vulgaris* that contains rubredoxin centers and a hemerythrin-like binuclear iron cluster. Biochemistry. 1988;**27**:1636-1642

[130] Sundaramoorthy M, Kishi K, Gold MH, Poulos TL. The crystal structure of manganese peroxidase from *Phanerochaete chrysosporium* at 2.06-Å resolution. Journal of Biological Chemistry. 1994;**269**:32759-32767

[131] Dismukes GC. Manganese enzymes with binuclear active sites. Chemical Reviews. 1996;**96**:2909-2926. DOI: 10.1021/cr 950053c

[132] Pace RJ, Stranger R, Petrie S. Why nature chose Mn for the water oxidase in photosystem II. Dalton Transactions. 2012;**41**:7179-7189. DOI: 10.1039/ c2dt30185g

[133] Renirie R, Hemrika W, Wever R. Peroxidase and phosphatase activity of active-site mutants of vanadium chloroperoxidase from the fungus *Curvularia inaequalis*: Implications for the catalytic mechanisms. Journal of Biological Chemistry. 2000;**275**: 11650-11657. DOI: 10.1074/ jbc.275.16.11650

[134] Liu S, Lu F, Xing R, Zhu JJ. Structural effects of Fe_3O_4 nanocrystals on peroxidase-like activity. Chemistry (Weinheim an der Bergstrasse, Germany). 2011;**17**:620-625. DOI: 10.1002/chem.201001789

[135] Dong J, Song L, Yin J-J, He W, Wu Y, Gu N, et al. Co_3O_4 nanoparticles with multi-enzyme activities and their application in immunohistochemical assay. ACS Applied Materials & Interfaces. 2014;**6**:1959-1970. DOI: 10.1021/am405009f

[136] Hayman AR, Cox TM. Purple acid phosphatase of the human macrophage and osteoclast. Characterization, molecular properties, and crystallization of the recombinant di-iron-oxo protein secreted by baculovirus-infected insect cells. Journal of Biological Chemistry. 1994;**269**:1294-1300

[137] Veljanovski V, Vanderbeld B, Knowles VL, Snedden WA, Plaxton WC. Biochemical and molecular characterization of AtPAP26, a vacuolar purple acid phosphatase up-regulated in phosphate-deprived Arabidopsis suspension cells and seedlings. Plant Physiology. 2006;**142**:1282-1293. DOI: 10.1104/pp.106.087171

[138] Cashikar AG, Kumaresan R, Madhusudhana Rao N. Biochemical characterization and subcellular localization of the red kidney bean purple acid phosphatase. Plant Physiology. 1997;**114**:907-915. DOI: 10.1104/pp.114.3.907

[139] Bozzo GG, Raghothama KG, Plaxton WC. Structural and kinetic properties of a novel purple acid phosphatase from phosphate-starved tomato (*Lycopersicon esculentum*) cell cultures. Biochemical Journal. 2004;**377**: 419-428. DOI: 10.1042/BJ20030947

[140] Feng C, Tollin G, Enemark JH. Sulfite oxidizing enzymes. Biochimica et Biophysica Acta—Proteins and Proteomics. 2007;**1774**:527-539. DOI: 10.1016/j.bbapap.2007.03.006

[141] Schwarz G, Mendel RR, Ribbe MW. Molybdenum cofactors, enzymes and pathways. Nature. 2009;**460**: 839-847. DOI: 10.1038/nature08302

[142] Wei H, Wang E. Nanomaterials with enzyme-like characteristics

(nanozymes): Next-generation artificial enzymes. Chemical Society Reviews. 2013;**42**:6060-6093. DOI: 10.1039/c3cs35486e

[143] Zhang K, Zuo W, Wang Z, Liu J, Li T, Wang B, et al. A simple route to $CoFe_2O_4$ nanoparticles with shape and size control and their tunable peroxidase-like activity. RSC Advances. 2015;**5**:10632-10640. DOI: 10.1039/C4RA15675G

[144] Baken S, Moens C, van der Grift B, Smolders E. Phosphate binding by natural iron-rich colloids in streams. Water Research. 2016;**98**:326-333. DOI: 10.1016/j.watres.2016.04.032

[145] Gottselig N, Nischwitz V, Meyn T, Amelung W, Bol R, Halle C, et al. Phosphorus binding to nanoparticles and colloids in forest stream waters. Vadose Zone Journal. 2017;**16**. DOI: 10.2136/vzj 2016.07.0064

[146] Leytem AB, Mikkelsen RL, Gilliam JW. Sorption of organic phosphorus compounds in Atlantic Coastal Plain soils. Soil Science. 2002;**167**:652-658. DOI: 10.1097/01.ss.0003034854.98442.39

[147] Celi L, Barberis E. Abiotic stabilization of organic phosphorus in the environment. In: Turner BL, Frossard E, Baldwin DS, editors. Organic Phosphorus in the Environment. Boston: Oxford University Press; 2005. pp. 113-132. DOI: 10.1079/9780851998220.0113

[148] Berg AS, Joern BC. Sorption dynamics of organic and inorganic phosphorus compounds in soil. Journal of Environmental Quality. 2006;**35**: 1855-1862. DOI: 10.2134/jeq2005.0420

[149] Ruttenberg KC, Sulak DJ. Sorption and desorption of dissolved organic phosphorus onto iron (oxyhydr)oxides in seawater. Geochimica et Cosmochimica Acta. 2011;**75**:4095-4112. DOI: 10.1016/j.gca.2010.10.033

[150] Wu J, Boyle E, Sunda W, Wen L-S. Soluble and colloidal iron in the oligotrophic North Atlantic and North Pacific. Science. 2001;**293**:847-849. DOI: 10.1126/science.1059251

[151] Li W, Liu D, Wu J, Kim C, Fortner JD. Aqueous aggregation and surface deposition processes of engineered superparamagnetic iron oxide nanoparticles for environmental applications. Environmental Science & Technology. 2014;**48**:11892-11900. DOI: 10.1021/es502174p

[152] Fitzsimmons JN, Bundy RM, Al-Subiai SN, Barbeau KA, Boyle EA. The composition of dissolved iron in the dusty surface ocean: An exploration using size-fractionated iron-binding ligands. Marine Chemistry. 2015;**173**: 125-135. DOI: 10.1016/j.marchem.2014.09.002

[153] Colombo C, Di Iorio E, Liu Q, Jiang Z, Barrón V. Iron oxide nanoparticles in soils: Environmental and agronomic importance. Journal of Nanoscience and Nanotechnology. 2017;**17**(7):4449-4460. DOI: 10.1166/jnn.2017.14197

[154] Golchin J, Golchin K, Alidadian N, Ghaderi S, Eslamkhah S, Eslamkhah M, et al. Nanozyme applications in biology and medicine: An overview. Artificial Cells, Nanomedicine, and Biotechnology. 2017;**45**:1069-1076. DOI: 10.1080/21691401.2017.1313268

[155] Zhou Y, Liu B, Yang R, Liu J. Filling in the gaps between nanozymes and enzymes: Challenges and opportunities. Bioconjugate Chemistry. 2017;**28**: 2903-2909. DOI: 10.1021/acs.bioconjchem.7b00673

[156] Singh R, Berry RE, Yang F, Zhang H, Walker FA, Ivancich A. Unprecedented peroxidase-like activity of *Rhodnius prolixus* nitrophorin 2:

Identification of the [FeIV=O por•]+ and [FeIV=O por](Tyr38•) intermediates and their role(s) in substrate oxidation. Biochemistry. 2010; **49**:8857-8872. DOI: 10.1021/bi100499a

[157] Wang H, Huang Y. Prussian-blue-modified iron oxide magnetic nanoparticles as effective peroxidase-like catalysts to degrade methylene blue with H2O2. Journal of Hazardous Materials. 2011;**191**:163-169. DOI: 10.1016/j.jhazmat.2011.04.057

[158] Liu B, Liu J. Accelerating peroxidase mimicking nanozymes using DNA. Nanoscale. 2015;**7**:13831-13835. DOI: 10.1039/C5NR04176G

[159] Zhang Z, Zhang X, Liu B, Liu J. Molecular imprinting on inorganic nanozymes for hundred-fold enzyme specificity. Journal of the American Chemical Society. 2017;**139**:5412-5419. DOI: 10.1021/jacs.7b00601

[160] Fan K, Wang H, Xi J, Liu Q, Meng X, Duan D, et al. Optimization of Fe_3O_4 nanozyme activity via single amino acid modification mimicking an enzyme active site. Chemical Communications. 2017;**53**:424-427. DOI: 10.1039/c6cc08542c

[161] Fox TR, Comerford NB. Rhizosphere phosphatase activity and phosphatase hydrolyzable organic phosphorus in two forested spodosols. Soil Biology and Biochemistry. 1992;**24**: 579-583. DOI: 10.1016/0038-0717(92)90083-A

[162] McLatchey GP, Reddy KR. Regulation of organic matter decomposition and nutrient release in a wetland soil. Journal of Environmental Quality. 1998;**27**:1268-1274. DOI: 10.2134/jeq1998.00472425002700050036x

[163] Hoppe HG. Phosphatase activity in the sea. Hydrobiologia. 2003;**493**: 187-200. DOI: 10.1023/A:1025453918247

[164] Turner BL, McKelvie ID, Haygarth PM. Characterisation of water-extractable soil organic phosphorus by phosphatase hydrolysis. Soil Biology and Biochemistry. 2002;**34**:27-35. DOI: 10.1016/S0038-0717(01)00144-4